# Photoinduced electron transfer and photodegradation of malonic acid at Au/TiO$_2$ investigated by in situ ATR-IR spectroscopy

Xuefeng Hu [a,c,*], Thomas Bürgi [b,c,*]

[a] Key Laboratory of Coastal Zone Environmental Processes, Yantai Institute of Coastal Zone Research, Chinese Academy of Sciences, Yantai Shandong 264003, PR China
[b] Département de Chimie Physique, Quai Ernest-Ansermet 30, 1211 Genève 4, Switzerland
[c] Physikalisch Chemisches Institut, Ruprecht-Karls-Universität Heidelberg, Im Neuenheimer Feld 253, 69120 Heidelberg, Germany

## ABSTRACT

TiO$_2$ coated Au nanoparticles were synthesized and characterized by TEM, XPS and XRD. It was found that the Au nanoparticles were coated with TiO$_2$ thus forming a core–shell structure. Electron transfer, adsorption and photodegradation of malonic acid on the catalyst were investigated by in situ attenuated total reflection infrared (ATR-IR) spectroscopy. Malonic acid adsorbed and underwent photodegradation efficiently in air and nitrogen atmosphere under UV light illumination on the prepared catalyst. As intermediate species oxalate was observed on the catalyst surface during the photodegradation of malonic acid. The Au nanoparticles accelerate the degradation of malonic acid by capturing the conduction band electrons of TiO$_2$. The ATR spectra also reveal interface electron transfer from Au nanoparticles to TiO$_2$ under visible light illumination and from TiO$_2$ to Au nanoparticles under UV illumination.

© 2012 Elsevier B.V. All rights reserved.

## 1. Introduction

Photocatalytic reactions over TiO$_2$ play an essential role in many applications, such as the degradation of organic pollutants, water splitting, CO$_2$ reduction and solar cells [1,2]. A photocatalytic reaction is initiated by electron–hole pair generation upon band gap excitation. The low photon efficiency of the photocatalytic process largely arises from electron–hole recombination processes. Therefore, much effort has been devoted to efficiently separate the electron–hole pair. The use of metal-semiconductor heterostructures is a popular strategy for applications in photocatalysis because the metal in contact with the semiconductor greatly enhances the overall photocatalytic redox process [3–5]. However, corrosion or dissolution of the noble metal nanoparticles occurring during photocatalytic reactions is a challenge [6,7]. Heterostructures with a Au nanoparticle core and a TiO$_2$ shell would be a good candidate as stable photocatalyst since the TiO$_2$ shell may reduce the corrosion of the metal.

Although attenuated total reflection infrared (ATR-IR) spectroscopy has been applied for some time in various fields of research, its application in heterogeneous catalysis has gained significant attention only recently, mainly because of its promising features for in situ investigation of catalytic solid-liquid interfaces [8]. Notwithstanding the technique's potential has been demonstrated, its application to study photocatalytic degradation of organic pollutants are still quite limited in number. ATR-IR has been used in the past to study the fate of organic molecules adsorbed on the TiO$_2$ surface upon UV exposure [9,10]. We investigated the adsorption and UV light photocatalytic degradation routs of dicarboxylic acids at TiO$_2$ [11–13]. It was for example shown that succinic acid is converted to malonic acid, which is then converted to oxalic acid and finally to CO$_2$. By using selectively $^{13}$C labeled malonic acid it was also shown that malonic acid decomposition via oxalate is only one possible pathway, accounting for about 50% of the malonic acid conversion. The photocatalysis of amino acids at TiO$_2$ modified with Au nanoparticles was also studied by us [6] with particular emphasis on the fate of the nitrogen atom. As most important finding it was shown that under certain reaction conditions cyanide is formed, which can adsorb on the gold and even lead to leaching the latter. ATR-IR has also been used to study the band gap irradiation of TiO$_2$ particle films in contact with water [14]. Vibrational bands below 1000 cm$^{-1}$ that appeared upon UV illumination were first assigned to surface peroxo or hydroperoxo

* Corresponding authors at: Key Laboratory of Coastal Zone Environmental Processes, Yantai Institute of Coastal Zone Research, Chinese Academy of Sciences, Yantai Shandong 264003, PR China. Tel.: +86 535 2109157/41 0 22 3796552; fax: +86 535 2109157.
*E-mail addresses:* xfhu@yic.ac.cn (X. Hu), Thomas.Buergi@unige.ch (T. Bürgi).

species [15]. Subsequent transmission IR work on $TiO_2$ in quasi-vacuum conditions by Yamakata et al. [16] and Szczepankiewicz et al. [17] suggested electronic transitions from shallow traps or intra-conduction band as the origin of the observed signals in the infrared spectra [16]. Warren and McQuillan [14] confirmed the shallow trap explanation using ATR-IR spectroscopy. The trapped electrons were consumed by the recombination with holes and also by transfer to other electron acceptors. Tracing trapped electrons in the semiconductor can give valuable information that can be used for the better understanding of the photocatalytic reactivity of the catalyst.

In the present study, $TiO_2$ coated Au nanoparticles were synthesized. ATR-IR spectroscopy was used to monitor the absorption corresponding to the presence of shallow electron traps, as well as the organic molecules adsorbed on the surface of the heterostructure catalyst. Electron acceptors accelerate the photodegradation of organic molecules on $TiO_2$. The interface electron transfer from Au nanoparticles to $TiO_2$ under visible light illumination and from $TiO_2$ to Au nanoparticles under UV illumination revealed the potential applications of the catalyst in photoreduction and photooxidation reactions, which has already been demonstrated for the oxidation of thiols and the reduction of disulfides [18].

## 2. Experimental

### 2.1. Chemicals

All chemicals were purchased from Sigma–Aldrich and were used as received. All solutions were prepared using Milli-Q water (18.2 MΩ cm). Nitrogen ($N_2$, 99.995%) and oxygen ($O_2$, 99.995%) both from CarbaGas, were applied to saturate the liquids.

### 2.2. Preparation of the Au@TiO$_2$ catalyst

*Au nanorod preparation:* For the growth solution, 250 mL of CTAB (0.2 M) was pipetted into a 1 L round-bottomed flask, constantly stirred through the use of a magnetic stirrer bar and kept at 27 °C in an oil bath. 12.5 mL of fresh $AgNO_3$ (4 mM) was added, followed by 250 mL of room temperature $HAuCl_4$ (1 mM) solution. Three minutes after the addition of the Au, 3.5 mL of ascorbic acid (78.8 mM) was measured into the flask. The seed solution was prepared by adding 5 mL $HAuCl_4$ (0.5 mM) to 5 mL CTAB (0.2 M) in a 50 mL round-bottomed flask. 0.6 mL of freshly prepared, ice-cold $NaBH_4$ was introduced whereupon the solution was stirred for a further two minutes before stopping the stirring for five minutes. At this point 0.8 mL of the seed solution was introduced into the growth solution and the reaction was left to continue until completion (typically around twelve hours).

*Au@TiO$_2$ preparation:* 10 mg titanium (IV) oxide acetylacetonate was added into 10 mL Au nanorod solution and stirred using a magnetic stirrer bar at room temperature for 10 h. The resulting solid was centrifuged and washed with water, then dried at 80 °C. Pure $TiO_2$ as a reference material was prepared directly by hydrolysis of titanium (IV) oxide acetylacetonate in CTAB aqueous solution.

### 2.3. Thin-film preparation and catalyst characterization

Thin films of the catalyst were prepared by suspending 10 mg of Au@TiO$_2$ or $TiO_2$ catalyst in 10 mL of Milli-Q water. The slurry was sonicated for 30 min. The thin film was formed by dropping the slurry onto a Ge internal reflection element (IRE, 52 mm × 20 mm × 1 mm; KOMLAS). The solvent was evaporated at 30 °C, and the procedure was repeated three times. After drying for several minutes at 30 °C in air, loose catalyst particles were removed by flowing water over the IRE. Then the sample was heated
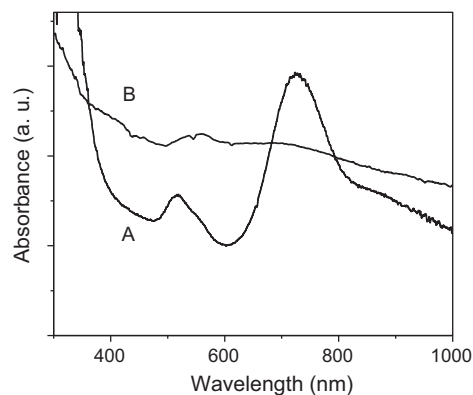


**Fig. 1.** UV–vis absorption of catalyst (A) dried at 80 °C and (B) calcined at 450 °C for 12 h.

at 80 °C or 450 °C for 12 h. For every experiment a fresh catalyst film was prepared in the same way.

For the UV-vis spectroscopy, thin films were prepared according to the same method but with glass as the substrate. X-ray diffraction (XRD) of the sample was done on a PANalytical X'Pert PRO MPD system using Cu Kα radiation. Transmission electron microscopy was carried out by using a CM200 Transmission Electron Microscope operating at 200 kV acceleration voltage. Chemical analysis was performed by the energy dispersive X-ray technique. X-ray photoelectron spectroscopy (XPS) data were recorded using a Mg Kα X-ray source and a LHS 11 analyzer. The spectra acquisition was carried out in normal emission geometry with an energy resolution of 0.9 eV. The X-ray source was operated at a power of 260 W and positioned 1.5 cm away from the samples.

### 2.4. In situ ATR-IR spectroscopy

ATR spectra were recorded with a dedicated flow-through cell as reported before [6]. Briefly, the flow-through cell was made from a Teflon piece, a fused silica plate (45 mm × 35 mm × 3 mm) with holes for in and outlet (36 mm apart), and a flat (1 mm) viton seal. Multiple reflection Ge internal reflection elements (IRE, 52 mm × 20 mm × 1 mm; KOMLAS) were used at an angle of incidence of 45°. The cell was mounted on an attachment for ATR measurements within the sample compartment of a Bruker Equinox-55 FTIR spectrometer equipped with a narrow-band MCT detector. Spectra were recorded at 4 cm$^{-1}$ at room temperature. Two hundred scans were accumulated for each spectrum. For irradiation of the sample UV light from the source (75 W Xe arc lamp) was guided to the cell via two fiber bundles. Filters from ITOS were used to obtain light in the range of 270–380 nm and >570 nm, respectively, for UV light and visible light excitation, respectively.

## 3. Results and discussion

### 3.1. Characterization of the Au@TiO$_2$ catalyst

The visible absorption spectra of Au@TiO$_2$ films both before and after calcination at 450 °C for 12 h were clearly characterized by the plasmon resonance peaks of Au nanoparticles as shown in Fig. 1. The Au nanorods (Fig. 2a) before calcinations showed two bands: a strong band at ca. 700 nm corresponding to electron oscillations along the long axis, and a band at ca. 520 nm corresponding to electron oscillations along the short axis [19]. The strong absorbance band at ca. 700 nm decreased after calcinations at 450 °C, indicating the disappearance of the Au nanorods, which is also confirmed by the TEM images in Fig. 2b. Au nanoparticles were coated with $TiO_2$ thus forming a core–shell structure from the TEM images
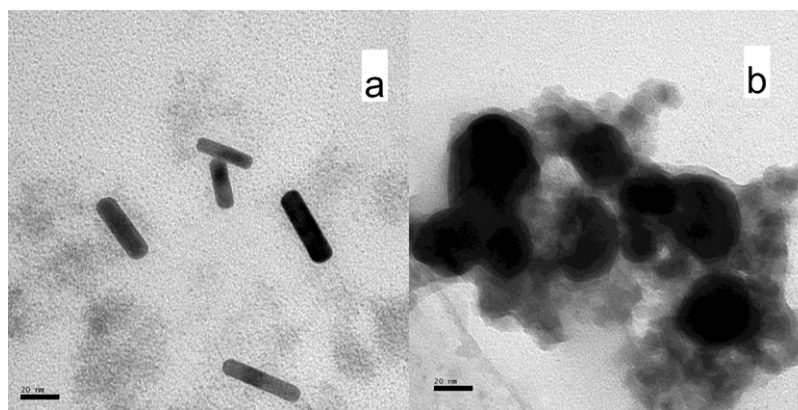
**Fig. 2.** TEM images of catalyst (a) dried at 80 °C and (b) calcined at 450 °C for 12 h. The scale bar is 20 nm.

(Fig. 2b). A TiO$_2$ layer thickness of about 4 nm is estimated although pure TiO$_2$ nanoparticles around the core–shell structure blurred the interface. Also, even after calcination the Au particles were not spherical, reminiscent of the initial nanorods. This leads to multiple plasmon resonances for individual particles and therefore a broad extinction band over the visible spectral range for the sample. Energy-dispersive X-ray (EDX) analysis showed that TiO$_2$ and Au is present in the dark parts of the image but only TiO$_2$ and no Au is found in the bright parts (Fig. s1).

To verify the state of Ti and Au in the catalyst, XPS were measured (Fig. 3). The peaks observed at 84.0 and 87.7 eV reveal metallic gold due to the Au nanoparticles [20], and the peaks at 459.2 and 465.0 eV are characteristic for Ti$^{4+}$ [21]. XRD was used to investigate the crystallographic phase of the catalyst (Fig. s2). The major crystalline phase of TiO$_2$ was anatase and the Au nanoparticles showed a cubic phase.

### 3.2. Carboxylic acid adsorption and photodegradation intermediates

Au@TiO$_2$ heated at 80 °C showed catalytic activity for the degradation of malonic acid. However, the degradation of other organic compounds introduced during the preparation process resulted in complex IR spectra (Fig. s3). Therefore, the catalyst heated to 450 °C was used for the IR study of malonic acid degradation. Fig. 4 shows (a) malonic acid and (c) oxalic acid adsorbed on the Au@TiO$_2$ from air-saturated aqueous solution in the dark. The most intense bands of malonate are assigned to carboxylate vibrations $\nu_{as}$(COO) at 1595 and $\nu_s$(COO) at 1427 cm$^{-1}$, respectively [11,22]. This shows that malonic acid adsorbed on Au@TiO$_2$ in deprotonated form, i.e. as malonate, and the spectrum furthermore indicates that the two carboxylate groups are equivalent because only one

set of carboxylate vibrations is observed. The wavenumber difference ($\Delta$) between the $\nu_{as}$(COO) and $\nu_s$(COO) modes is diagnostic for the coordination mode of the carboxylate [22]. If $\Delta$ for the adsorbed carboxylate is larger than for the corresponding dissolved species, a monodentate coordination mode is indicated. A smaller $\Delta$ for the adsorbed species than for the dissolved ones is characteristic for chelating and/or bridging coordination. For malonate adsorbed on the Au@TiO$_2$ catalyst a $\Delta$ value of 168 cm$^{-1}$ is found, which is smaller than the value of the dissolved species (209 cm$^{-1)}$) and thus a chelating or bridging adsorption mode is proposed for the malonate as shown in our previous research [12]. The spectrum of the most strongly adsorbed oxalated species showed a band at 1690 cm$^{-1}$ and a shoulder at 1710 cm$^{-1}$. Furthermore the same species exhibited a band at 1408 cm$^{-1}$ and a weaker one at 1263 cm$^{-1}$. The bands at 1408 cm$^{-1}$ and 1263 cm$^{-1}$ are therefore assigned to $\nu$(C—O) + $\nu$(C—C) and $\nu$(C—O) + $\nu$(O—C=O) vibrations [23,24]. The appearance of two bands around 1700 cm$^{-1}$ reveals two groups with C=O character, and the two distinct vibrational bands in the spectrum correspond to the symmetric and antisymmetric C=O stretching vibration [11]. Trace (b) in Fig. 4 shows the ATR spectrum after the adsorbed malonate illuminated with UV light for 10 min. Positive absorbance bands of oxalate at 1710, 1690, 1408 and 1263 cm$^{-1}$ can be observed and the negative ones at 1595 and 1427 cm$^{-1}$ are associated with malonate that is removed from the catalyst surface. This indicates that malonic acid photodegradation occurred upon UV illumination with oxalate formed as intermediate.

The adsorption kinetics of malonic acid in the dark was found to be similar on TiO$_2$ and on Au@TiO$_2$ as can be seen from Fig. 5. After about 6 min adsorption was almost complete and the ATR-IR spectra of malonate on the two catalysts was very similar. Also the signal intensity at adsorption equilibrium was almost the same (see
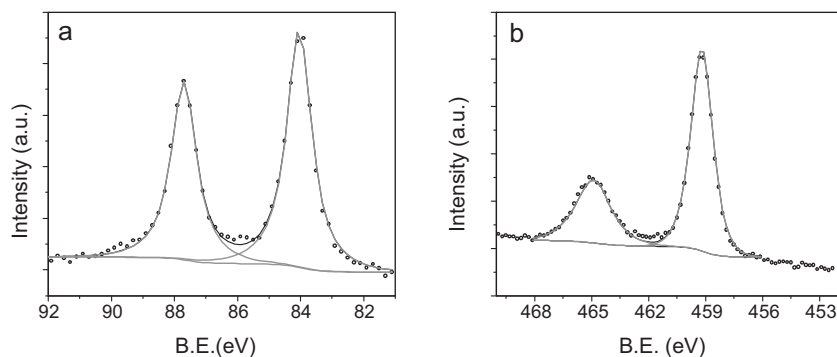


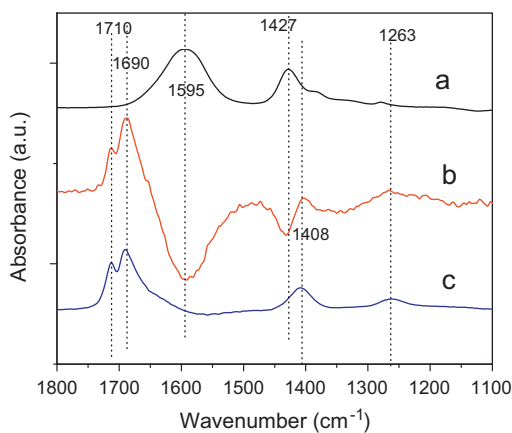**Fig. 3.** X-ray photoelectron spectroscopy (XPS) of (a) Au and (b) Ti in the catalyst.

**Fig. 4.** ATR-IR spectra of (a) malonic acid, (c) oxalic acid adsorbed on Au@TiO$_2$ in the dark. Spectrum (b) represents the spectral change observed after malonic acid adsorption on Au@TiO$_2$ and ten minutes UV light illumination with the solution flow stopped (with the dark adsorbed spectrum as background). The spectra were adjusted to similar absorbance intensity for comparison.



**Fig. 6.** ATR-IR spectra related to malonic acid photodegradation. Spectra (a) and (b) were obtained after 28 min UV illumination over TiO$_2$ under air atmosphere and Au@TiO$_2$ under nitrogen atmosphere while flowing malonic acid ($3 \times 10^{-4}$ M), respectively. The background was collected after 28 min malonic acid adsorption before illumination. Spectrum (c) was obtained with (b) as background and after exposing the sample to O$_2$-saturated solution for 28 min.

inset in Fig. 5). This indicates that the TiO$_2$ has similar properties for both catalysts and that the Au nanoparticles are covered by TiO$_2$ in the Au@TiO$_2$ case.

### 3.3. Photodegradation and electron transfer on Au@TiO$_2$ during UV illumination

Electron–hole pairs are created when the TiO$_2$ catalyst is illuminated by UV light, however, they readily recombine in the absence of local trap states and/or an electric field promoting their separation. On the one hand, small molecular carboxylic acids usually provide a hole trapping pathway, which reduces surface recombination and facilitate the persistence of electrons, allowing them to migrate to shallow traps of about 0.1 eV below the conduction band edge [25]. On the other hand, electron acceptors provide an electron capture pathway, which can reduce surface recombination and increase the persistence of the holes, allowing them to oxidize adsorbed species [26]. The presence of electron acceptors also reduces the migration of electron to shallow traps.

Both malonic acid on bare TiO$_2$ in the presence of air-saturated water and malonic acid on Au@TiO$_2$ in the presence of nitrogen-saturated water showed photodegradation under UV illumination as shown in Fig. 6a and b. Oxygen acts as the electron acceptor in the TiO$_2$ case, which leads to an increased lifetime of the
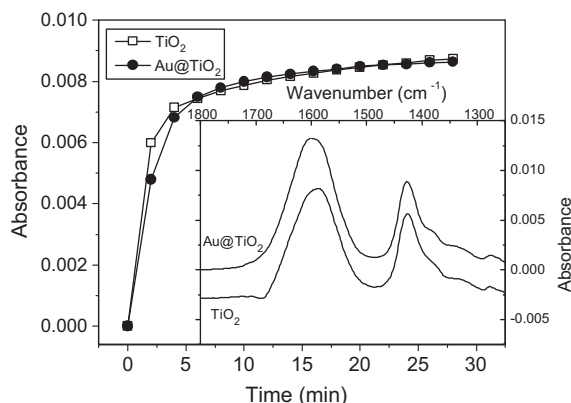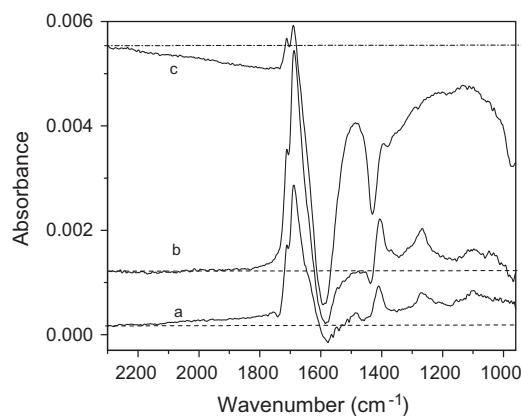
photogenerated hole and the generation of reactive oxygen species from the reduced oxygen. The hole and the reactive oxygen species can oxidize the malonic acid directly. However, there is no oxygen acting as electron acceptor in the Au@TiO$_2$ case (Fig. 6b). In the latter case the Au nanoparticles act as the electron acceptor and therefore promote the electron–hole pair separation and photodegradation of malonic acid. The degradation rates of oxalic acid on TiO$_2$ and Au@TiO$_2$ were measured to investigate the catalytic activity of the two catalysts. The Au@TiO$_2$ catalyst showed higher catalytic activity (Fig. 7). The stronger positive absorbance signals of the oxalate intermediate and negative absorbance signals of adsorbed malonate in the Au@TiO$_2$ case compared to the TiO$_2$ case as shown in Fig. 6 also verified this. This indicates that Au nanoparticles are good acceptors of TiO$_2$ conduct band electrons.

When the Au@TiO$_2$ reaction system was subsequently exposed to oxygen for another 28 min under UV illumination, the negative bands of the malonate increased quickly. It is clear that oxygen, as an electron acceptor, takes photo-excited electrons from the Au nanoparticles directly or via TiO$_2$ so as to increase the photodegradation of malonic acid. However, the negative absorption bands of malonate increased much more than the positive absorption bands of oxalate as shown in Fig. 6c. This indicates that oxygen changes the relative rates of malonate oxidation, oxalate formation and oxalate oxidation. We had pointed out before that the transformation of malonic acid into oxalic acid may not be the only
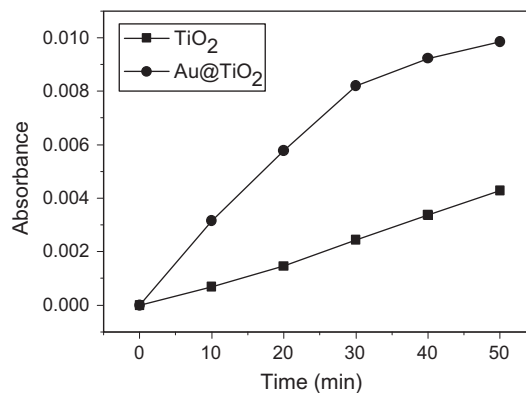


**Fig. 5.** Time profile of the absorbance of malonate at $1427\,\text{cm}^{-1}$ on TiO$_2$ and Au@TiO$_2$ with $3 \times 10^{-4}$ M malonic acid aqueous solution flowing over the catalyst film. (Inset) The inset shows ATR-IR spectra of adsorbed malonate on TiO$_2$ and Au@TiO$_2$ after 28 min adsorption in the dark.



**Fig. 7.** Time profile of the negative absorbance of oxalate at $1710\,\text{cm}^{-1}$ during UV light illumination. The background collected after 28 min oxalic acid adsorption ($3 \times 10^{-4}$ M) before illumination. The solution flow stopped during illumination.

pathway of malonic acid photodegradation in air [12]. Malonate photodegradation is initiated by injection of a hole (photo-Kolbe reaction), which results in the elimination of $CO_2$ [12]. Subsequent steps lead from the carbon-centered radical to a carboxylate [11]. There are at least two pathways leading from the carbon-centered radical to the oxalate. The two pathways are characterized by different oxygen sources, dissolved oxygen and oxygen from water. Reactive species formed from oxygen play a key role in turning the carbon-centered radical to a carboxylate and therefore oxalate. In addition to that, in the presence of oxygen, the lifetime of the hole increases. The overall effect of this is a faster rate of malonate oxidation in the presence of oxygen. In contrast, the photocatalytic mineralization of oxalate performs mainly through the hole oxidation mechanism. The ratio of the oxalate signals (positive) and the malonate signals (negative) depend on the kinetics of the different oxidation mechanisms. The experiments (Fig. 6b and c) showed that oxygen accelerates the removal of malonate with respect to the formation of oxalate. It can be deduced that the overall reaction rate of malonic acid photo-assisted degradation may be larger due to other possible pathways involving oxygen that do not go through oxalic acid.

The presence of malonic acid provides a hole trap and electrons can be transferred to these acceptors or traps located in the midgap shallow states of $TiO_2$. The shallow trapped electrons show a broad absorption, extending from above 2000 to below 1000 $cm^{-1}$ with increasing intensity at lower wavenumbers. No electrons are trapped in the midgap shallow states if the excited electrons are completely transferred to electron acceptors during the UV illumination and the broad IR absorption will not be observed. In our experiments a broad IR absorption of trapped electrons in the $TiO_2$ case during UV illumination in air was evidenced (Fig. 6a), which was even stronger in $N_2$ atmosphere (not shown). However, we cannot see this absorption in the Au@$TiO_2$ case in air atmosphere (not shown), and even in $N_2$ atmosphere as shown in Fig. 6b. This further shows that Au nanoparticles in the catalyst act as an efficient electron acceptor and thus eliminate electrons trapped in the midgap shallow states. When the Au@$TiO_2$ sample in $N_2$ atmosphere was exposed to oxygen, a strong negative broad absorption appeared as shown in Fig. 6c. This indicates that some electrons, trapped in the midgap shallow state in nitrogen atmosphere can be captured by the oxygen. The decreased number of shallow trapped electrons indicates that more electrons transfer to electron acceptors and therefore more holes are left to oxidize adsorbed species. Overall this leads to an increased photodegradation rate of adsorbed organic compounds. In this case, the broad IR absorption due to trapped electrons [14] can be regarded as an indicator of electron–hole pair separation and organic pollutant photodegradation efficiency.

### 3.4. Visible light induced electron transfer

Au nanoparticles are of great interest due to their plasmon resonance giving rise to their color varieties in the visible spectral range. The visible light absorption can be observed in our Au@$TiO_2$ sample even though the Au nanoparticles are wrapped with $TiO_2$ because the $TiO_2$ shell is transparent in the visible region. In the infrared the Au@$TiO_2$ sample showed a strong broad absorption band above 1000 $cm^{-1}$ under visible light illumination as shown in Fig. 8a. The addition of $Fe^{3+}$ to visible light illuminated Au@$TiO_2$ caused an abrupt decrease of this absorption and an increase of the negative malonate signal as shown in Fig. 8b. $Fe^{3+}$ is reported to be an efficient acceptor of $TiO_2$ conduct band electrons [27]. The decrease of the broad absorption due to trapped electrons can therefore be assigned to the migration of trapped electrons to $Fe^{3+}$. Upon visible light illumination electrons are transferred from the excited Au particles to the $TiO_2$ conduction band, and then some of the
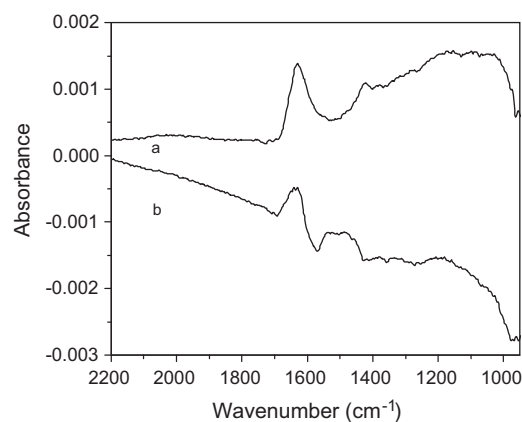


**Fig. 8.** ATR-IR spectra recorded during visible light illumination of adsorbed malonic acid: (a) illuminated with visible light above 570 nm for 53 min (the background collected after 28 min malonic acid adsorption in the dark) while flowing malonic acid ($3 \times 10^{-4}$ M) over the Au@$TiO_2$ catalyst, (b) 14 min after addition of $6 \times 10^{-4}$ M $FeCl_3$ to the flowing malonic acid solution.

electrons are trapped in the midgap shallow states. There is no evident oxalate formation observed during visible light illumination as shown in Fig. 8a. The hole left in the Au cannot oxidize malonate efficiently [20]. The visible light excited electrons transferred to $Fe^{3+}$ to form $Fe^{2+}$ can also be transferred to $O_2$ to form reactive oxygen species such as $H_2O_2$. The photogenerated $Fe^{2+}$ and $H_2O_2$ may result in the decrease of adsorbed malonate. The visible light illumination also caused an increase of the water band at 1630 $cm^{-1}$, which may be due to the visible light induced wettability change of the catalyst [28,29].

It is also known that Au nanoparticles can be efficiently heated upon illumination [30]. In order to check if the observations could be explained by a heating effect some additional experiments were performed. We observed that changing the sample solution from 25 to 70 °C also caused an absorbance around 1000 $cm^{-1}$. However, when $FeCl_3$ was added to the heated solution, the absorbance kept increasing (Fig. s4). This suggests that the strong absorbance around 1000 $cm^{-1}$ from the illuminated Au@$TiO_2$ catalyst is the result of the trapped electrons and not due to a temperature effect.

## 4. Conclusion

In situ ATR-IR is a useful tool for the investigation of heterogeneous photocatalytic reactions and interface electron transfer of $TiO_2$-containing heterostructures. The Au nanoparticles, embedded in the catalyst, act as electron acceptor and promote the degradation of malonic acid even in the absence of oxygen under UV light illumination. Oxalate as intermediate product can be observed on the catalyst surface during the photodegradation. Visible light excited Au nanoparticles transfer electrons to the conduction band of $TiO_2$ and some of the electrons are trapped in the midgap shallow states. The trapped electrons can be captured by $Fe^{3+}$. Thus, the catalyst showed potential for applications in photoreduction/photooxidation reactions using visible light/UV light illumination.

## Appendix A. Supplementary data

Supplementary data associated with this article can be found, in the online version, at http://dx.doi.org/10.1016/j.apcata.2012.09.017.

## References

[1] X.B. Chen, S.S. Mao, J. Catal. 107 (2007) 2891–2959.
[2] P. Usubharatana, D. Mcmartin, A. Veawab, P. Tontiwachwuthikul, Ind. Eng. Chem. Res. 45 (2006) 2558–2568.
[3] Q. Zhang, D.Q. Lima, I. Lee, F. Zaera, M. Chi, Y. Yin, Angew. Chem. Int. Ed. 123 (2011) 7226–7230.
[4] K. Awazu, M. Fujimaki, C. Rockstuhl, J. Tominaga, H. Murakami, Y. Ohki, N. Yoshida, T. Watanabe, J. Am. Chem. Soc. 130 (2008) 1676–1680.
[5] H. Tada, T. Kiyonaga, S. Naya, Chem. Soc. Rev. 38 (2009) 1849–1858.
[6] I. Dolamic, T. Burgi, J. Phys. Chem. C 115 (2011) 2228–2234.
[7] P.V. Kamat, J. Phys. Chem. C 111 (2007) 2834–2860.
[8] T. Burgi, A. Baiker, Adv. Catal. 50 (2006) 227–283.
[9] P.Z. Araujo, C.B. Mendive, L.A. Garcia Rodenas, P.J. Morando, A.E. Regazzoni, M.A. Blesa, D. Bahnemann, Colloids Surf. A: Physicochem. Eng. Aspects 265 (2005) 73–80.
[10] A.R. Almeida, J.A. Moulijn, G. Mul, J. Phys. Chem. C 112 (2008) 1552–1561.
[11] I. Dolamic, T. Burgi, J. Catal. 248 (2007) 268–276.
[12] I. Dolamic, T. Burgi, J. Phys. Chem. B 110 (2006) 14898–14904.
[13] I. Dolamic, Molecular Insight into Photocatalytic Reactions by TiO2 Investigated by ATR-IR Spectroscopy, PhD Thesis, Université de Neuchâtel, 2008.
[14] D.S. Warren, A.J. McQuillan, J. Phys. Chem. B 108 (2004) 19373–19379.
[15] R. Nakamura, A. Imanishi, K. Murakoshi, Y. Nakato, J. Am. Chem. Soc. 125 (2003) 7443–7450.
[16] A. Yamakata, T. Ishibashi, H. Onishi, Chem. Phys. Lett. 333 (2001) 271–277.
[17] S.H. Szczepankiewicz, A.J. Colussi, M.R. Hoffmann, J. Phys. Chem. B 104 (2000) 9842–9850.
[18] S. Naya, M. Teranishi, T. Isobe, H. Tada, Chem. Commun. 46 (2010) 815–817.
[19] S.S. Chang, C.W. Shih, C.D. Chen, W.C. Lai, C.R. Chris Wang, Langmuir 15 (1999) 701–709.
[20] Y. Tian, T. Tatsuma, J. Am. Chem. Soc. 127 (2005) 7632–7637.
[21] B. Erdem, R.A. Hunsicker, G.W. Simmons, E.D. Sudol, V.L. Dimonie, M.S. El-Aasser, Langmuir 17 (2001) 2664–2669.
[22] S.J. Hug, D. Bahnemann, J. Electron Spectrosc. Relat. Phenom. 150 (2006) 208–219.
[23] A.G. Young, A.J. McQuillan, Langmuir 25 (2009) 3538–3548.
[24] A.D. Weisz, L. Garcia Rodenas, P.J. Morando, A.E. Regazzoni, M.A. Blesa, Catal. Today 76 (2002) 103–112.
[25] D.M. Savory, D.S. Warren, A.J. McQuillan, J. Phys. Chem. C 115 (2011) 902–907.
[26] A.L. Linsebigler, G.J.T. Lu Jr., Chem. Rev. 95 (1995) 735–758.
[27] G.R. Bamwenda, T. Uesigi, Y. Abe, K. Sayama, H. Arakawa, Appl. Catal. A: Gen. 205 (2001) 117–128.
[28] Y. Abdi, M. Khalilian, E. Arzi, J. Phys. D: Appl. Phys. 44 (2011) 255405–255410.
[29] Y. Tian, H. Notsu, T. Tatsuma, Photochem. Photobiol. Sci. 4 (2005) 598–601.
[30] H.H. Richardson, Z.N. Hickman, A.O. Govorov, A.C. Thomas, W. Zhang, M.E. Kordesch, Nano Lett. 6 (2006) 783–788.